# Orbital and spin orderings in $YVO_3$ and $LaVO_3$ in the generalized gradient approximation

Hideaki Sawada and Noriaki Hamada
*Joint Research Center for Atom Technology, Angstrom Technology Partnership, 1-1-4 Higashi, Tsukuba, Ibaraki 305, Japan*

Kiyoyuki Terakura
*Joint Research Center for Atom Technology, National Institute for Advanced Interdisciplinary Research, 1-1-4 Higashi, Tsukuba, Ibaraki 305, Japan*

Toshio Asada
*Faculty of Liberal Arts, Shizuoka University, Hamamatsu, Shizuoka 432, Japan*
(Received 21 July 1995; revised manuscript received 12 December 1995)

The orbital and spin orderings of $d^2$ Jahn-Teller systems are studied in the generalized gradient approximation (GGA) by using the full-potential linearized augmented-plane-wave method. For the low temperature distorted crystal structures in $YVO_3$ and $LaVO_3$ perovskites, we show that orbital orderings and insulating band structures are obtained properly in GGA, but are not in the local spin density approximation. Bond length alternations in the $ab$ plane cause the $C$-type and $G$-type orderings of $d_{yz}$ and $d_{zx}$ orbitals, which in turn stabilize the $G$-type and $C$-type antiferromagnetic spin orderings in $YVO_3$ and $LaVO_3$, respectively. The total energy calculation partially confirms the relation between orbital and spin orderings, and indicates that the extent of the orbital ordering is still insufficient for $YVO_3$ in GGA. [S0163-1829(96)09619-1]

## I. INTRODUCTION

The transition-metal (TM) oxides with the perovskite-type structure $AMO_3$ ($A$ being alkali earth metals, lanthanides, and so on, and $M$ being $3d$ TM elements) form a very important group of materials possessed of several characteristic properties. The dielectric property combined with the structural phase transition such as ferroelectricity is one of such characteristic properties and remarkable progress has been made recently in the theoretical study in this respect.[1–3] The success of such a study may be due to the following two aspects: first, the related materials are simple band insulators; second, the key quantity in the theoretical study is the total energy change associated with deformation of the atomic arrangement. These two aspects are very favorable to the local density approximation (LDA) in the density functional theory, making the theoretical studies mentioned above a prototypical example of the success of LDA.

The situation becomes very different for the materials which exhibit interesting magnetic and transport properties. Several experimental works have been recently performed, particularly on giant magnetic resistance,[4,5] and we have started systematic studies of related materials with La or Y as $A$ and Ti-Cu as $M$.[6,7] In this case, the formal charge of $M$ is $3^+$ and the $d$ band is partially occupied. Therefore, the materials may be regarded as strongly correlated systems and skepticism exists about the applicability of LDA and the local spin density approximation (LSDA). However, we have demonstrated in our previous papers[6,7] that most of the ground state properties as well as the single-electron excitation spectra of $LaMO_3$ with $M$=Mn-Ni can be described reasonably well by the LSDA band calculation. We argued the reasons why the perovskite TM oxides are better described by LSDA compared with TM oxides with the rock-salt structure. Nevertheless, we also noticed that the LSDA band calculations cannot reproduce the band gap for $LaMO_3$ with M=Ti, V, and Co. It is therefore obvious that we have to go beyond LSDA in order to deal with $LaMO_3$ ($M$=Ti-Ni) properly in a unified way. It is an important subject to study what level of approximation is necessary to describe at least the ground state properties properly for this category of materials.

In the present work, we take $LaVO_3$ and $YVO_3$ as two examples of the materials whose insulating ground state cannot be reproduced by the LSDA calculations. We demonstrate that both systems become insulating in the generalized gradient approximation (GGA) though the band gaps are significantly underestimated. The important point is that with the crystal structure given by experiment GGA stabilizes the orbital ordering associated with the Jahn-Teller distortion. Singh and Pickett reported that the gradient correction moves $CaCuO_2$ towards an experimentally obtained insulating antiferromagnetic solution but that the correction is too small to produce an instability of the paramagnetic ground state.[8] The enhancement of the orbital ordering by GGA was first pointed out by Dufek *et al.*[9] for CoO and FeO. The crystal structure is different between $LaVO_3$ and $YVO_3$ and accordingly the type of the orbital ordering is also different between them. By the analogy of the spin ordering in the antiferromagnetic states, we call the orbital ordering of $LaVO_3$ ($YVO_3$) the $G$ type ($C$ type). We then discuss that the $G$-type ($C$-type) orbital ordering is responsible for the stability of the $C$-type ($G$-type) antiferromagnetic spin ordering of $LaVO_3$ ($YVO_3$). In the density functional theory, it is of primary importance for the band calculation to reproduce the insulating or metallic nature of the ground state properly. The band gap is always underestimated significantly. In this sense, the GGA calculation is a definite improvement over the LSDA calculation for $LaVO_3$ and $YVO_3$. Nevertheless, the present work also shows that GGA still has a serious

 

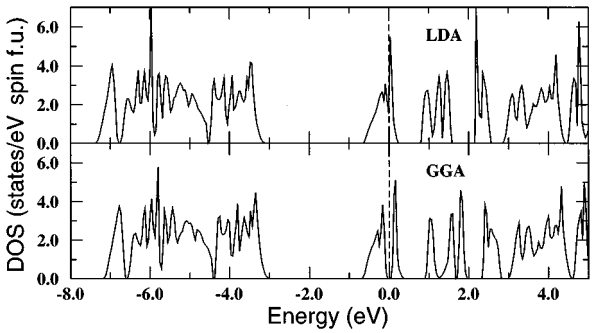


FIG. 1. Total DOS for the $G$-type AF $YVO_3$ in the orthorhombic structure.

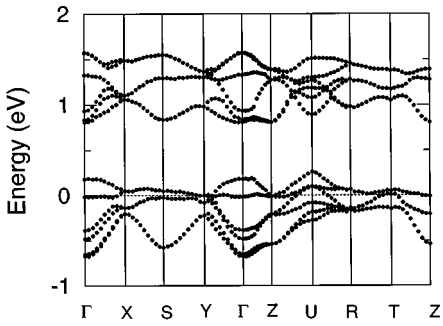


FIG. 2. Band structure for the $G$-type AF $YVO_3$ in the orthorhombic structure calculated in LSDA.

problem in reproducing the lowest energy structure properly for $YVO_3$, probably because the calculated orbital ordering is insufficient.

## II. CALCULATIONAL METHOD

The electronic structure calculations are performed by using the full-potential linearized augmented-plane-wave (FLAPW) method. For the exchange-correlation energy in LSDA, an analytical expression of Vosko, Wilk, and Nusair is employed.[10] For gradient correction to the exchange-correlation energy, the GGA proposed by Perdew and Wang[11,12] is used. The muffin-tin sphere radii of lanthanum, yttrium, vanadium, and oxygen are chosen to be 1.43, 1.38, 1.06, and 0.85 Å, respectively. The angular momentum in the spherical-wave expansion is truncated at $l_{\max}=6$ and 7 for the potential and the wave function, respectively. The energy cutoff of the plane wave is 12 Ry for the wave function. In these calculations 8 **k** points are used in the irreducible Brillouin zone, which correspond to 27 **k** points in the first Brillouin zone, and the linear tetrahedron method is employed to sum up the occupied states.

## III. RESULTS

### A. $YVO_3$

$YVO_3$ has orthorhombic perovskite structure with space group $Pbnm$, and the lattice parameters are $a=5.279$, $b=5.589$, and $c=7.548$ Å at 56 K.[13] The spin structure of this compound is $G$-type antiferromagnetic (AF) below 77 K, $C$-type AF between 77 and 118 K, and paramagnetic above 118 K. An anomaly in the lattice constants is observed at 77 K, while any structural anomaly has not been observed at 118 K. The magnetic moments are 1.6 and $1.0\mu_B$ for the $G$-type and $C$-type AF phases, respectively. $YVO_3$ is an insulator with an activation energy of 0.25 eV (Ref. 14) and an optical gap of 1.2 eV.[15]

The total density of states (DOS) for $YVO_3$ calculated in LSDA and GGA are shown in Fig. 1. The O $2p$ states are located below $-3.0$ eV: the V $d\varepsilon$ ($t_{2g}$) states are split by the intra-atomic exchange interaction, and are located from $-0.7$ eV to 0.3 eV and from 0.8 eV to 1.6 eV in LSDA. The exchange splitting is estimated to be 1.3 eV in LSDA, which increases to 1.5 eV in GGA, because the magnetic moment inside the V muffin-tin sphere increases from $1.36\mu_B$ in LSDA to $1.45\mu_B$ in GGA. The magnetic moment is in fairly good agreement with the experimental value of $1.6\mu_B$.[13] Figure 1 shows an important difference between LSDA and GGA: $YVO_3$ is metallic in LSDA, while it is insulating with the fundamental band gap of 0.09 eV and the direct gap of 0.27 eV in GGA. Though the calculated fundamental and direct gaps are smaller than the corresponding experimental ones,[14,15] it should be noted that the existence of the gap itself is important in the density functional theory even though the value of the band gap is not necessarily well reproduced. Figures 2 and 3 clearly show the similarity and the difference between the band structures of LSDA and GGA. The twelve $d\varepsilon$ bands split into lower six bands and upper six bands due to the intra-atomic exchange interaction. The important difference between LSDA and GGA is that the whole bandwidth of the six bands is wider in GGA, while the bandwidth of each single band is narrower in GGA. This makes peaks of DOS more prominent and produces a band gap at the Fermi level in GGA. The appearance of the energy gap in GGA is due to an orbital ordering caused by a lattice distortion as explained below.

The V atom is octahedrally surrounded by six O atoms. The V atom is located at the center of the inversion symmetry, and the three types of V-O bond pairs have directions of approximately [110], [110], and [001]. Two of them are short and have almost the same length (1.98 Å), while the other is long (2.05 Å) and lies in the $ab$ plane. These bonds are arranged in such a way as shown in Fig. 4. The long-bond pairs whose directions are indicated by arrows are parallel to each other along the $c$ axis, and alternately arranged in the $ab$ plane. This bond arrangement is called the $C$ type in this paper by analogy of the spin ordering.

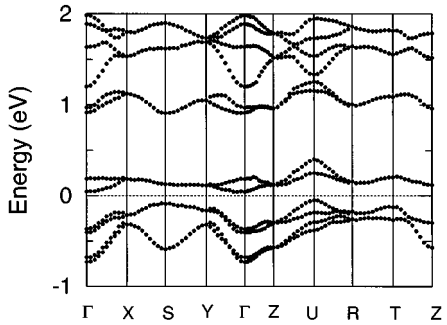


FIG. 3. Band structure for the $G$-type AF $YVO_3$ in the orthorhombic structure calculated in GGA.

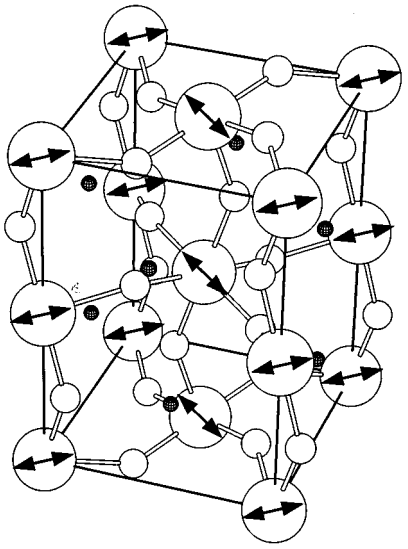

FIG. 4. The bond arrangement in $YVO_3$. The largest sphere denotes V, the middle one O, and the smallest one Y. The directions of the longest bonds are shown by arrows: one is approximately [110] direction and the other is approximately [110] direction. This bond arrangement is called the *C*-type arrangement.

Figures 5, 6, and 7 show the charge density contours produced by the occupied $d\varepsilon$ bands. Figure 5 shows the charge density contour plot in the (001) plane containing the V atoms. All the V sites in the plane are equivalent, that is, the neighboring V sites are connected by 180° screw rotation along the [100] axis. The $d_{xy}$ orbital is occupied at every V site with the $x$ and $y$ axes taken in the [110] and [110] directions, respectively. The $d_{xy}$ orbital forms a $\pi$ bond with the O $2p_x$ or $2p_y$ orbitals, more strongly for the shorter bond, although the $\pi$ bond charge is not seen so clearly in Fig. 5 because the O atom is slightly off the $ab$ plane.

Figure 6 shows the charge density contour plot in the (110) plane containing the V atoms. In this plane, the charge densities of V atoms aligned in the [001] direction are equivalent. However, the V atoms along line $b$ have much higher charge densities than the ones along line $a$: the $d_{yz}$ orbital is preferentially occupied at the V site along line $b$ which has a long-bond pair in the $y$ direction, namely, the [110] direction. A similar situation is seen in the (110) plane, as shown in Fig. 7. The $d_{zx}$ orbital is preferentially occupied at the V site along the line $a'$ which has a long-bond pair in the $x$ direction, namely, the [110] direction. Note that line $a$ ($b$) in Fig. 6 is equivalent to line $a'$ ($b'$) in Fig. 7. Thus, the $d_{zx}$ and $d_{yz}$ orbitals are preferentially occupied at the V atoms along lines $a$ and $b$, respectively. These charge densities indicate that the *C*-type orbital ordering occurs in $YVO_3$ due to the alternation of the bond length in the $ab$ plane.

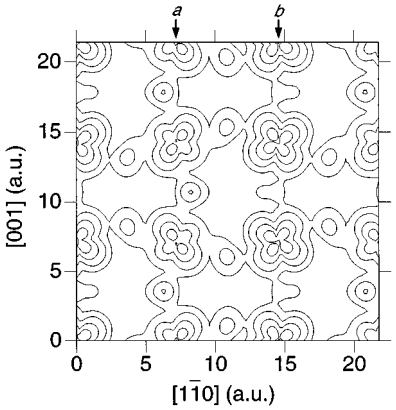


FIG. 6. The charge density contour plot in the (110) plane containing the V atoms for the *G*-type AF $YVO_3$ in the orthorhombic structure calculated in GGA. Contour values are $1.56\times10^{-3}$, $6.25\times10^{-3}$, $2.50\times10^{-2}$, and $1.00\times10^{-1}e$/a.u.$^3$.

### B. $LaVO_3$

$LaVO_3$ undergoes orthorhombic-to-monoclinic structural phase transition at 140 K accompanied with a paramagnetic-to-antiferromagnetic phase transition as temperature decreases.[16] The low temperature phase is monoclinic with the following lattice parameters: $a=5.5917$, $b=5.5623$, $c=7.7516$ Å, $\alpha=90.129°$, and space group $P2_1/b$. In contrast to $YVO_3$ there are two inequivalent V sites in

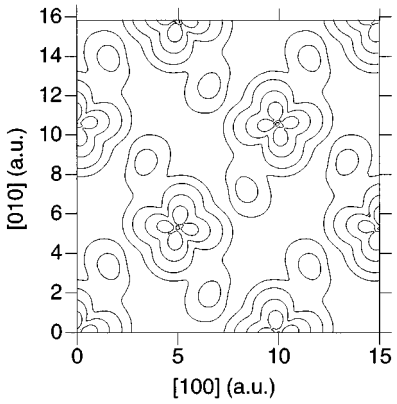


FIG. 5. The charge density contour plot in the (001) plane containing the V atoms for the *G*-type AF $YVO_3$ in the orthorhombic structure calculated in GGA. Contour values are $1.56\times10^{-3}$, $6.25\times10^{-3}$, $2.50\times10^{-2}$, and $1.00\times10^{-1}e$/a.u.$^3$.

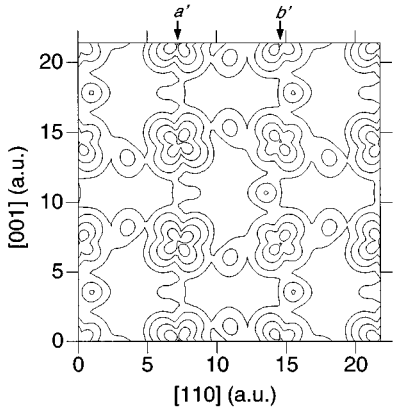


FIG. 7. The charge density contour plot in the ($1\bar{1}0$) plane containing the V atoms for the *G*-type AF $YVO_3$ in the orthorhombic structure calculated in GGA. Contour values are $1.56\times10^{-3}$, $6.25\times10^{-3}$, $2.50\times10^{-2}$, and $1.00\times10^{-1}e$/a.u.$^3$.

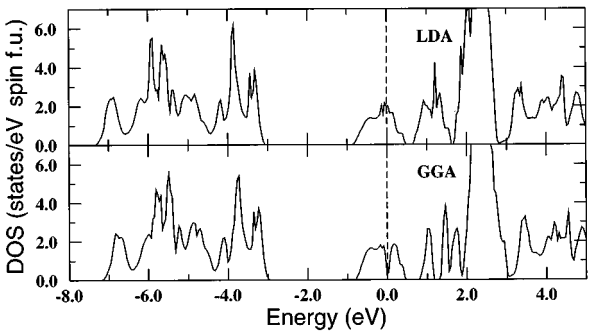


FIG. 8. Total DOS for the $C$-type AF $LaVO_3$ in the monoclinic structure.

$LaVO_3$, which are stacked along the $c$ axis. Neutron diffraction measurement shows that the $C$ type of AF spin ordering occurs and the magnetic moment of a V atom is $1.3\mu_B$.[17,18] $LaVO_3$ is an insulator with an activation energy of about 0.2 eV (Refs. 19 and 20) and an optical gap of 1.1 eV.[15]

Figure 8 shows the total DOS calculated in LSDA and GGA. The energy regions of the O $2p$ and the V $3d$ states are almost the same as those in $YVO_3$. The O $2p$ states are located from $-8.3$ eV to $-3.0$ eV: the V $d\varepsilon$ ($t_{2g}$) states are located from $-0.8$ eV to 0.5 eV and from 0.6 eV to 1.7 eV in LSDA. The exchange splitting is 1.3 eV in LSDA, while it increases to 1.4 eV in GGA. The magnetic moment obtained in GGA is $1.47\mu_B$, which is larger than that in LSDA (i.e., $1.38\mu_B$). Considering that these magnetic moments are evaluated in the rather small muffin-tin sphere with the radius of 1.06 Å, we may judge that they are too large in comparison with the experimental value of $1.3\mu_B$.[17,18] On the other hand, the calculated magnetic moment is smaller than the experimental one in $YVO_3$. Furthermore, the previous work shows that the calculated magnetic moments are smaller than the experimental values for $LaCrO_3$, $LaMnO_3$, and $LaFeO_3$.[6] The discrepancy of the magnetic moment in $LaVO_3$ may be removed by taking account of the orbital moment, which may be induced by the difference in the occupation between $m=1$ and $m=-1$ orbitals. It is expected that the orbital moment may be larger in $LaVO_3$ than in $YVO_3$, because six $d\varepsilon$ bands are split into four and two

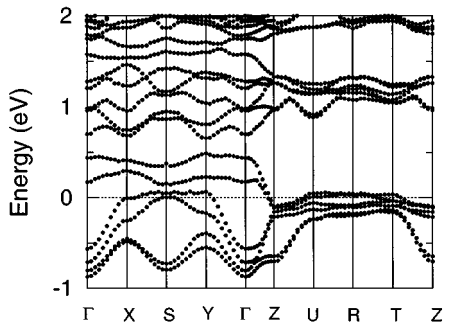


FIG. 9. Band structure for the $C$-type AF $LaVO_3$ in the monoclinic structure calculated in LSDA. The orthorhombic **k**-point indices are taken, because the monoclinic distortion is very small and the Brillouin zone is almost the same as the orthorhombic one.

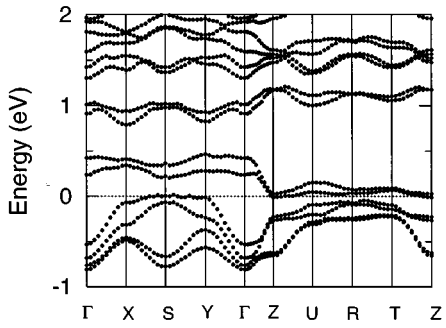


FIG. 10. Band structure for the $C$-type AF $LaVO_3$ in the monoclinic structure calculated in GGA.

bands completely in $YVO_3$, while this splitting is not complete in $LaVO_3$. Further investigation, however, is needed to check this point. Figures 9 and 10 show the twelve $d\varepsilon$ bands in LSDA and GGA, respectively. The whole width of six $d\varepsilon$ bands in $LaVO_3$ is 0.3 eV larger than that in $YVO_3$. The bond angle of V-O-V of $LaVO_3$ is in the range $156.1°-157.8°$, which is much larger than that of $YVO_3$ ($144.3°-144.8°$), leading to the wider $d\varepsilon$ bands in $LaVO_3$. $LaVO_3$ is metallic in LSDA, while it is almost insulating in GGA. The fundamental gap is very close to zero, and the optical gap is 0.1 eV in GGA. Although the band gaps are smaller than the experimental values, the existence of the band gap is essential to obtain appropriate charge and spin densities which are the most fundamental quantities in the density functional theory. The appearance of the band gap is a result of an orbital ordering also in $LaVO_3$, but the type of its orbital ordering is different from the one in $YVO_3$ as described below.

The arrangement of long (2.04 Å) and short (1.98 Å) V-O bond pairs of $LaVO_3$ is different from that of $YVO_3$, and it causes a different orbital ordering between $LaVO_3$ and $YVO_3$. As shown in Fig. 11, if a V atom has a long-bond pair in the [110] direction, all six neighbor V atoms have long-bond pairs in the [110] direction. This bond arrangement is called the $G$ type. In this monoclinic structure there

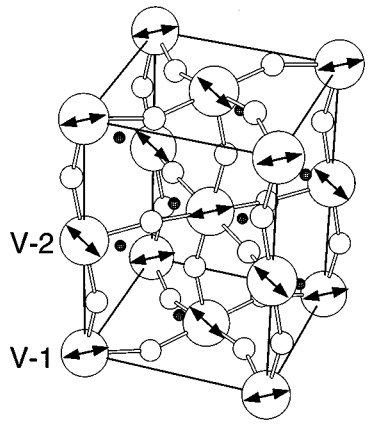


FIG. 11. The bond arrangement in $LaVO_3$. The largest sphere denotes V, the middle one O, and the smallest one La. V-1 and V-2 denote two inequivalent V atoms. The directions of the longest bonds are shown by arrows: one is approximately [110] direction and the other is approximately [110] direction. This bond arrangement is called the $G$-type arrangement.

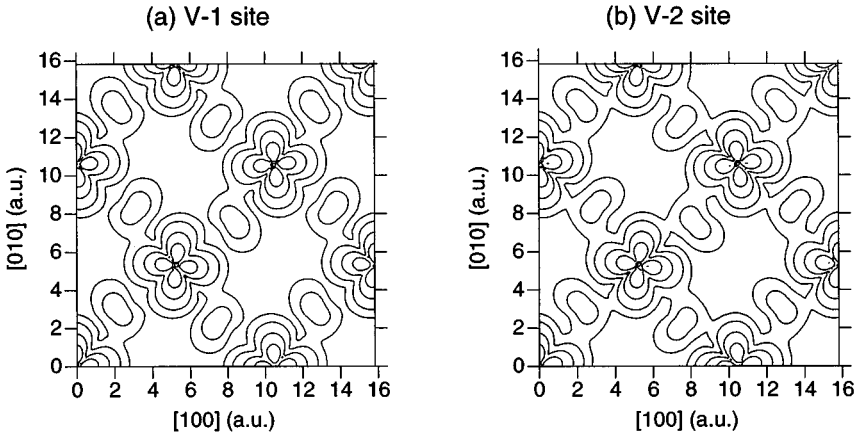


FIG. 12. The charge density contour plots in the (001) plane including (a) V-1 and (b) V-2 sites for the *C*-type AF $LaVO_3$ in the monoclinic structure calculated in GGA. Contour values are $1.56\times10^{-3}$, $6.25\times10^{-3}$, $2.50\times10^{-2}$, and $1.00\times10^{-1}e$/a.u.$^3$.

are two inequivalent V sites (V-1 and V-2 in Fig. 11) which are stacked along the *c* axis. Although these two V sites have slightly different V-O bond lengths, this difference is very small and not important for the orbital ordering.

Figures 12, 13, and 14 show the charge density contours produced by the occupied $d\varepsilon$ bands. Figures 12(a) and (b) show charge density contour plots in adjacent (001) planes including the V sites. The charge densities of the adjacent planes are almost the same, although the oxygen positions are slightly different between these two layers. All the V sites are equivalent in a plane, that is, neighboring V sites are connected by 180° screw rotation along the [100] axis. The $d_{xy}$ orbital is occupied at every V site, with the *x* and *y* axes taken in the [110] and [1$\bar{1}$0] directions, respectively. The $d_{xy}$ orbital forms a $\pi$ bond with the O $2p_x$ or $2p_y$ orbital, more strongly for the shorter bond. These features are almost the same as those in $YVO_3$.

Figure 13 shows the charge density contour plot in the (110) plane including the V sites. In this plane neighboring V atoms have significantly different charge densities: the $d_{yz}$ orbital is preferentially occupied in the V atoms which have a long-bond pair in the *y* direction, namely, the [110] direction. A similar situation is seen in the (110) plane, as shown in Fig. 14. The $d_{zx}$ orbital is preferentially occupied in the V atoms which have a long-bond pair in the *x* direction, namely, the [110] direction. Note that line *a* (*b*) in Fig. 13 is equivalent to line *a*′ (*b*′) in Fig. 14. These charge densities show the *G*-type orbital ordering in contrast to the *C*-type one in $YVO_3$.

### C. Stability of the spin ordering

The total energies are calculated in GGA for various spin orderings, i.e., *A*-type AF, *C*-type AF, *G*-type AF, and ferromagnetic spin orderings. The total energies of $YVO_3$ and $LaVO_3$ for these spin orderings are listed in Table I. In $YVO_3$, *G*-type AF has the highest energy, in disagreement with the experiment. In $LaVO_3$, however, the experimentally obtained *C*-type AF has the lowest energy. It is more difficult to predict the experimental spin ordering in $YVO_3$ than that in $LaVO_3$ for reasons given below. The bond angle of V-O-V of $YVO_3$ is smaller than that of $LaVO_3$ by 12° as mentioned above. It leads the 3*d* electrons of V to be more localized in $YVO_3$ than in $LaVO_3$, which is confirmed by seeing that the $d\varepsilon$ band width of $YVO_3$ is smaller than that of $LaVO_3$. The energy differences among these spin orderings are expected to be smaller in $YVO_3$ than in $LaVO_3$, since the localization of the 3*d* electrons of V makes exchange interaction coefficient *J* smaller. It is consistent with the experimental results that the antiferromagnetic transition

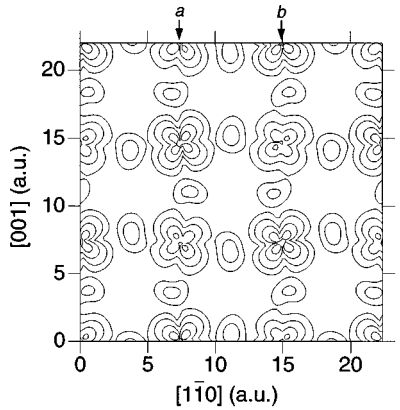


FIG. 13. The charge density contour plot in the (110) plane containing the V atoms for the *C*-type AF $LaVO_3$ in the monoclinic structure calculated in GGA. Contour values are $1.95\times10^{-3}$, $7.81\times10^{-3}$, $3.13\times10^{-2}$, and $1.25\times10^{-1}e$/a.u.$^3$.

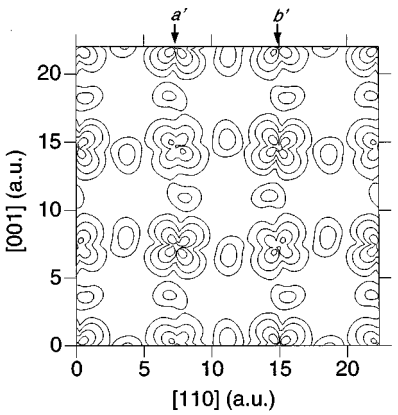


FIG. 14. The charge density contour plot in the ($1\bar{1}0$) plane containing the V atoms for the *C*-type AF $LaVO_3$ in the monoclinic structure calculated in GGA. Contour values are $1.95\times10^{-3}$, $7.81\times10^{-3}$, $3.13\times10^{-2}$, and $1.25\times10^{-1}e$/a.u.$^3$.

temperature of $YVO_3$ is lower than that of $LaVO_3$. GGA as well as LSDA will give worse results for more localized electron systems. The failure in $YVO_3$ and the success in $LaVO_3$ in reproducing the experimental spin ordering will be discussed further in the next section from a viewpoint of the relation between orbital and spin orderings. The incorrect prediction of the *C*-type AF in $YVO_3$ is related to the insufficient orbital ordering in the GGA calculation. The spin coupling along the *c* axis strongly depends on the degree of the ordering of the $d_{yz}$ and $d_{zx}$ orbitals, while the spin coupling in the *ab* plane is rather insensitive to such orbital orderings because of the dominant contribution of the $d_{xy}$ orbital (see the next section).

To summarize the results in Table I, in both $YVO_3$ and $LaVO_3$, ferromagnetic and *C*-type AF orderings in which spins couple ferromagnetically along the *c* axis are stabler than other cases like *A*-type and *G*-type AF. It implies that the ferromagnetic spin ordering is more favorable along the *c* axis. In the *ab* plane the energy differences between the ferromagnetic and antiferromagnetic couplings are not large in comparison with those along the *c* axis.

TABLE I. Total energies (meV/unit formula) of various spin orderings measured from the experimentally obtained one.

| | $YVO_3$ | $LaVO_3$ |
|---|---|---|
| Ferromagnetic | −17 meV | 35 meV |
| *A*-type AF | −6 meV | 44 meV |
| *C*-type AF | −18 meV | 0 meV |
| *G*-type AF | 0 meV | 52 meV |

## IV. DISCUSSION

In the previous sections, we have shown that the *C*-type and *G*-type orbital orderings occur in $YVO_3$ and $LaVO_3$, respectively. In this section, we will discuss qualitatively that these orbital orderings stabilize the *G*-type and *C*-type spin orderings in $YVO_3$ and $LaVO_3$, respectively. Figures 15, 16, and 17 show schematic site-projected partial DOS's at neighboring V sites whose spins couple (a) ferromagnetically and (b) antiferromagnetically. We consider hybridization between two neighboring V $d\varepsilon$ states through an O $p\pi$ state. The hybridization between occupied and unoccupied states lowers the energy of the occupied state by approximately $t^2/\Delta$, where $t$ is an effective transfer integral and $\Delta$ is an energy difference between the occupied and unoccupied states. We will discuss which spin coupling, namely, ferromagnetic or antiferromagnetic, is stabler in the *z* and *x* directions, respectively, from the viewpoint of the energy gain by the hybridization.

In $YVO_3$ there is no hybridization to produce an energy gain if the ferromagnetic coupling is assumed between the adjacent atoms in the *z* direction, since the same orbital, either $d_{zx}$ or $d_{yz}$, is occupied at these atoms [Figs. 6, 7, and 15(a)]. On the other hand, the antiferromagnetic coupling produces an energy gain through the hybridizations between $d_{zx}$ orbitals [Fig. 15(b)]. Therefore the energy gain by the hybridization favors antiferromagnetic coupling in the *z* direction. It is consistent with the *G*-type AF spin ordering observed in $YVO_3$. One should note, however, that the above discussion is very much idealized. In reality the competition between the ferromagnetic and antiferromagnetic couplings may be more subtle. The deviation of the V-O-V angle from 180° produces hybridization across the Jahn-Teller splitting even in the ferromagnetic coupling case. An even more stronger effect is produced by incomplete ordering of $d_{zx}$ and $d_{yz}$ orbitals. This latter effect is overestimated in the present calculation, leading to the incorrect prediction of the ground state spin ordering of $YVO_3$. The comparison between the GGA and LSDA calculations supports this argument. In LSDA the *C*-type AF is stabler than the *G*-type AF by 44 meV, and this energy difference is much larger than that in GGA. Thus, the GGA calculation has a clear tendency of stabilizing the *G*-type AF ordering, though not sufficiently, compared with the LSDA calculation.

In $LaVO_3$, there are two hybridization paths in the *z* direction with energy gains both in the ferromagnetic [Fig. 16(a)] and antiferromagnetic [Fig. 16(b)] coupling cases. The energy denominators $\Delta$ in $t^2/\Delta$ are the Jahn-Teller and exchange splittings in the ferromagnetic and antiferromagnetic coupling cases, respectively. The former is smaller than the latter as shown in Fig. 8. Therefore, the ferromagnetic coupling is more favorable than the antiferromagnetic coupling

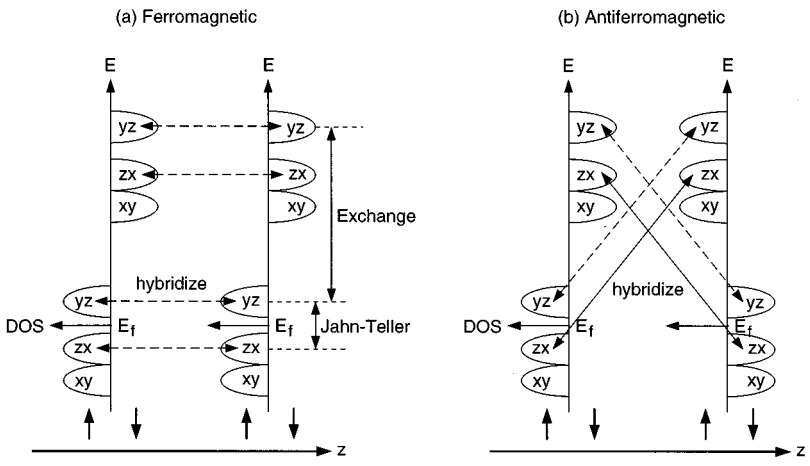


FIG. 15. Schematic site-projected partial DOS's in $YVO_3$ whose spins couple (a) ferromagnetically and (b) antiferromagnetically in the *z* direction. In $YVO_3$ either the $d_{yz}$ or the $d_{zx}$ orbital is occupied in V atoms aligned in the *z* direction. Hybridization paths producing energy gains are denoted by solid lines and those without energy gains by broken lines. The small hybridization between $d_{xy}$ orbitals is neglected.

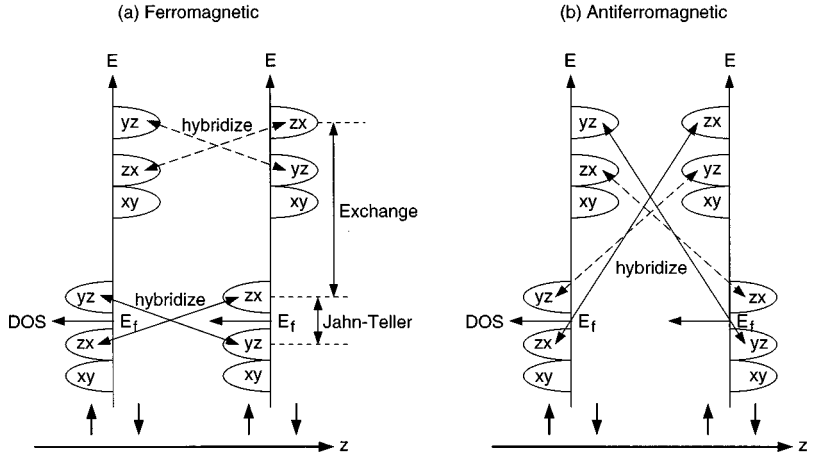


FIG. 16. Schematic site-projected partial DOS's in $LaVO_3$ whose spins couple (a) ferromagnetically and (b) antiferromagnetically in the $z$ direction. In $LaVO_3$ $d_{yz}$ and $d_{zx}$ orbitals are occupied alternately in the $z$ direction. Hybridization paths producing energy gains are denoted by solid lines and those without energy gains by broken lines. The small hybridization between $d_{xy}$ orbitals is neglected.

in the $z$ direction in $LaVO_3$. It is consistent with the $C$-type AF spin ordering obtained by neutron diffraction.[18] In this analysis incompleteness of the orbital ordering does not affect the stability of the spin ordering in $LaVO_3$, in contrast to $YVO_3$. This is the reason why GGA can reproduce the proper spin ordering in $LaVO_3$ in spite of the failure in $YVO_3$.

Now we discuss the situation in the $x$ direction as shown in Fig. 17; the situation in the $y$ direction is the same. It is not necessary to deal with $LaVO_3$ and $YVO_3$ separately, because these compounds have the same orbital and spin orderings in the $xy$ plane. In the ferromagnetic coupling case the occupied up-spin $d_{zx}$ orbital hybridizes with the unoccupied up-spin $d_{zx}$ orbital at the neighbor atom. In the antiferromagnetic coupling case there are three hybridization paths, namely, two paths for $d_{xy}$ orbitals and one for $d_{zx}$ orbitals. The $d_{yz}$-$d_{yz}$ hybridization is symmetrically allowed but must be small due to the small orbital overlap. If $t^2/\Delta$ in Fig. 17(a) with $\Delta$ the Jahn-Teller splitting is less than three times the corresponding one in Fig. 17(b) with $\Delta$ the exchange splitting, the antiferromagnetic spin ordering is realized. The experimental spin ordering is antiferromagnetic in the $xy$ plane both in $YVO_3$ and $LaVO_3$. Nevertheless, the above analysis suggests that the sign of the exchange coupling in the $xy$ plane may be delicate. It is consistent with the total energy calculations that the energy difference between the ferromagnetic and antiferromagnetic couplings in the $xy$ plane is smaller than that in the $z$ direction as mentioned in the previous section.

The close relation between the orbital and spin orderings is important to explain the relation between the antiferromagnetic transition and the crystallographic transition both in $LaVO_3$ and $YVO_3$. The antiferromagnetic transition and the crystallographic transition occur at the same temperature in $LaVO_3$. The Jahn-Teller distortion disappears above the transition temperature. It suggests that the orbital ordering and the spin ordering occur simultaneously in $LaVO_3$. In $YVO_3$, the magnetic transition from $G$-type to $C$-type AF with increasing temperature is accompanied with lattice distortion. One of the V-O bonds in the $ab$ plane is 3% larger than the others below the transition temperature. On the other hand, the two V-O bond lengths in the $ab$ plane become closer to each other and the V-O bond length in the $c$ axis is 2% shorter than those in the $ab$ plane above the transition temperature. This structural phase transition lowers the $d_{xy}$ orbital energy and makes the $d_{yz}$ and $d_{zx}$ orbital energies closer. The $d_{yz}$ and $d_{zx}$ orbitals are thereby almost equally occupied and the orbital ordering becomes weak. In the $z$ direction the hybridization across the Jahn-Teller splitting is enhanced by the weakening of the orbital ordering in the ferromagnetic coupling case. Thus, it stabilizes the ferromagnetic coupling in the $z$ direction above the transition

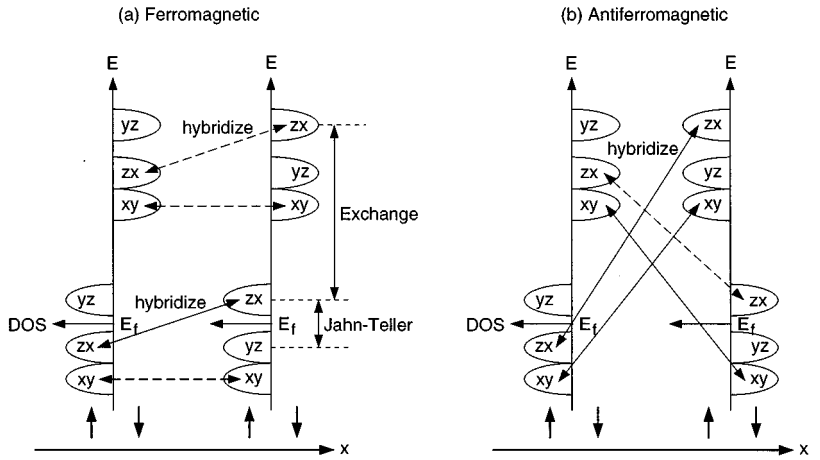


FIG. 17. Schematic site-projected partial DOS's whose spins couple (a) ferromagnetically and (b) antiferromagnetically in the $x$ direction. Hybridization paths producing energy gains are denoted by solid lines and those without energy gains by broken lines. The small hybridization between $d_{yz}$ orbitals is neglected.

temperature. In the $x$ direction the hybridization between the occupied and unoccupied $d_{zx}$ orbitals becomes weak both in the ferromagnetic and antiferromagnetic coupling because of the decrease in the occupancy of the $d_{zx}$ orbital. The antiferromagnetic coupling is still stable above the transition temperature, since the hybridization between the $d_{xy}$ orbitals plays a dominant role in lowering the energy. The $G$-type to $C$-type AF transition in $YVO_3$ can be qualitatively explained in this way. We can see that GGA predicts the experimentally second stabler spin ordering, namely, $C$-type AF, due to the insufficient orbital ordering.

## V. SUMMARY

The electronic structures of $YVO_3$ and $LaVO_3$ are calculated by the FLAPW method in LSDA and GGA. LSDA cannot yield insulating states for both of them, while GGA improves the LSDA results significantly. In GGA the complete insulating state is obtained for $YVO_3$, and $LaVO_3$ is almost insulating. The insulating states are closely related with the occurrence of the orbital ordering. The obtained orbital orderings are $C$ type and $G$ type for $YVO_3$ and $LaVO_3$, respectively. These orbital orderings strongly correlate with the V-O bond arrangement: the orbitals extending along the long V-O bond pair are preferentially occupied. A strong correlation has been pointed out between the spin and orbital orderings by considering the hybridization between the neighboring V $d\varepsilon$ states. This explains the simultaneous crystallographic and antiferromagnetic transition well both in $YVO_3$ and $LaVO_3$.

The GGA total energy calculations have shown that the $C$-type AF spin ordering has lowest energies both in $LaVO_3$ and $YVO_3$. Experimentally, this $C$-type AF phase is the lowest temperature phase in $LaVO_3$, while it is not in $YVO_3$. This partial failure of GGA is attributed to the insufficient orbital ordering in the GGA calculation.

## ACKNOWLEDGMENTS

The present work was partly supported by New Energy and Industrial Technology Development Organization (NEDO) and also by the Grant-in-Aid for Scientific Research from the Ministry of Education, Science and Culture of Japan.

[1] R. E. Cohen and H. Krakauer, Ferroelectrics **136**, 65 (1992).
[2] R. D. King-Smith and D. Vanderbilt, Phys. Rev. B **49**, 5828 (1994).
[3] W. Zhong, D. Vanderbilt, and K. M. Rabe, Phys. Rev. B **52**, 6301 (1995).
[4] Y. Tokura *et al.*, J. Mater. Sci. Eng. B **31**, 187 (1995).
[5] A. Urushibara *et al.*, Phys. Rev. B **51**, 14 103 (1995).
[6] N. Hamada, H. Sawada, and K. Terakura, in *Spectroscopy of Mott Insulators and Correlated Metals*, edited by A. Fujimori and Y. Tokura (Springer-Verlag, Berlin, 1995), p. 95.
[7] D. D. Sarma *et al.*, Phys. Rev. Lett. **75**, 1126 (1995).
[8] D. J. Singh and W. E. Pickett, Phys. Rev. B **44**, 7715 (1991).
[9] P. Dufek, P. Blaha, V. Sliwko, and K. Schwarz, Phys. Rev. B **49**, 10 170 (1994).
[10] S. H. Vosko, L. Wilk, and M. Nusair, Can. J. Phys. **58**, 1200 (1980).
[11] J. P. Perdew and Y. Wang, Phys. Rev. B **33**, 8800 (1986).
[12] J. P. Perdew, Phys. Rev. B **33**, 8822 (1986).
[13] H. Kawano, H. Yoshizawa, and Y. Ueda, J. Phys. Soc. Jpn. **63**, 2857 (1994).
[14] M. Kasuya *et al.*, Phys. Rev. B **47**, 6197 (1993).
[15] T. Arima, Y. Tokura, and J. B. Torrance, Phys. Rev. B **48**, 17 006 (1993).
[16] P. Bordet *et al.*, J. Solid State Chem. **106**, 253 (1993).
[17] V. G. Zubkov, G. V. Bazuev, V. A. Perelyaev, and G. P. Shveikin, Fiz. Tverd. Tela (Leningrad) **15**, 1610 (1973) [Sov. Phys. Solid State **15**, 1079 (1973)].
[18] V. G. Zubkov, G. V. Bazuev, and G. P. Shveikin, Fiz. Tverd. Tela (Leningrad) **18**, 2002 (1976) [Sov. Phys. Solid State **18**, 1165 (1976)].
[19] D. B. Rogers *et al.*, J. Appl. Phys. **37**, 1431 (1966).
[20] P. Dougier and P. Hagenmuller, J. Solid State Chem. **11**, 177 (1974).